MOLECULAR AND CELLULAR BIOLOGY, Sept. 1997, p. 5521–5529 Vol. 17, No. 9
0270-7306/97/$04.00+0

The *Drosophila bifocal* Gene Encodes a Novel Protein Which Colocalizes with Actin and Is Necessary for Photoreceptor Morphogenesis

SAMI M. BAHRI, XIAOHANG YANG, AND WILLIAM CHIA*

Institute of Molecular and Cell Biology, National University of Singapore, Singapore 119260

Received 4 April 1997/Returned for modification 10 May 1997/Accepted 21 June 1997

Photoreceptor cells of the *Drosophila* compound eye begin to develop specialized membrane foldings at the apical surface in midpupation. The microvillar structure ultimately forms the rhabdomere, an actin-rich light-gathering organelle with a characteristic shape and morphology. In a P-element transposition screen, we isolated mutations in a gene, *bifocal* (*bif*), which is required for the development of normal rhabdomeres. The morphological defects seen in *bif* mutant animals, in which the distinct contact domains established by the newly formed rhabdomeres are abnormal, first become apparent during midpupal development. The later defects seen in the mutant adult R cells are more dramatic, with the rhabdomeres enlarged, elongated, and frequently split. *bif* encodes a novel putative protein of 1063 amino acids which is expressed in the embryo and the larval eye imaginal disc in a pattern identical to that of F actin. During pupal development, Bif localizes to the base of the filamentous actin associated with the forming rhabdomeres along one side of the differentiating R cells. On the basis of its subcellular localization and loss-of-function phenotype, we discuss possible roles of Bif in photoreceptor morphogenesis.

The *Drosophila* eye has provided an excellent system with which to study pattern formation and differentiation at the single-cell level. The adult compound eye consists of ~800 unit eyes, or ommatidia, each containing eight photoreceptor neurons (R cells) and an invariant array of nonneuronal accessory cells. Each R cell projects to the center of the eye a microvillar stack of membranes rich in rhodopsin, called the rhabdomere (32). Rhabdomere position and size serve to distinguish between different classes of R cells.

Pattern formation in the developing *Drosophila* eye begins in the third instar larval eye disc and is closely associated with a morphological indentation in the disc called the morphogenetic furrow, which moves across the disc epithelium in a posterior-to-anterior direction (19). Differentiation of R cells initiates at the posterior edge of the furrow, and their formation is completed by the end of the third larval instar stage. In the midpupal stage (starting ~48 h postpuparium formation), R cells develop actin-rich microvillar structures (which will later form rhabdomeres) at the apical surface, a process normally characterized by disorganized membrane ruffling (29). At this stage, two distinct apical domains become apparent, a microvillar tip facing the future interretinal space and a smooth stalk extending to the adherens junctions (15). R7 projects to the center of the ommatidium and contacts surrounding rhabdomeres of other R cells. R3 builds its rhabdomere against the stalks of R2 and R4, whereas R4 forms contacts with the rhabdomeres of R2 and R7. Rhabdomere development is essentially completed at 110 h of pupation (prior to eclosion), by which stage they retract from the center of the retina, leaving behind an interretinal space.

At the subcellular level, the rhabdomeral microvilli are supported by an axial actin cytoskeleton and each microvillus contains a coalescence of at least two actin filaments (1) which extend from the distal ends of microvilli (barbed end of the filament) well into the cytoplasm of R cells (pointed end). Their pointed ends do not appear to be cross-linked in a "terminal web" fashion characteristic of the brush border microvilli (8, 17).

The microvillar rhabdomere of each R cell has its own characteristic position and shape and represents an interesting cellular subspecification for the study changes in cell morphology. Mutations that affect the normal rhabdomere structure usually result in a rough-eye phenotype. This class of mutations includes *chaoptin*, *calphotin*, *rdgc*, and *ninaC*. Chaoptin is a glycoprotein localized to the extracellular face of R-cell plasma membranes, and its mutation causes microvillar disorganization in developing rhabdomeres and disrupts the closely apposed membranes of adjacent R cells (28). Mutations in *calphotin*, which encodes an R-cell-specific calcium-binding protein, and *rdgC*, which encodes the calcium-binding serine/threonine protein phosphatase, have also been shown to cause structural alteration or misorientation of rhabdomeres (24, 34). In addition, mutations in *ninaC*, a gene encoding actin-based mechanoenzymes (kinase/myosin chimeras), result in fragmentation of the microvillar axial actin cytoskeleton and degeneration of the rhabdomeres (12).

In this paper, we describe the isolation and characterization of the gene *bifocal* (*bif*), which encodes a novel protein required for normal rhabdomere development in photoreceptor cells. Complete loss-of-function mutations in *bif* result in large, elongated, and frequently disrupted rhabdomeres. At the subcellular level, *bif* mutations affect actin distribution and disrupt the initial contact domains established by newly formed rhabdomeres. In addition, both the Bif and F-actin proteins colocalize at various developmental stages. The morphological defects associated with its loss of function and its subcellular localization suggest a requirement for the Bif protein in maintaining the shape and structural integrity of R-cell rhabdomeres.

* Corresponding author. Mailing address: Institute of Molecular and Cell Biology, National University of Singapore, 10 Kent Ridge Crescent, Singapore 119260. Fax: (65) 7791117. E-mail: mcbwchia@leonis.nus.sg.

MATERIALS AND METHODS

Standard molecular biology techniques were carried out as described by Sambrook et al. (21). Standard fly techniques were performed as described by Ashburner (2). The block and Prosite searches were carried out by using the MacPattern computer program as described by Fuchs (11).

Mutagenesis. *P842* and *P907* are two insertion lines carrying a P-element derivative, *P*[(w^+ ry^+)], that contains the *white* and *rosy* genes (14) inserted in the 10D region of the *Drosophila* X chromosome. The eye colors of these insertion lines are completely wild type (wt), and it was not possible to select for local transpositions on the basis of a change in eye color. The P elements in these lines were mobilized by using the immobile element *P*[ry^+ Δ*2-3*](*99B*) as a transposase source (20). Jump starter males of the genotype *P842* (or *P907*)/*Y*; *P*[ry^+ Δ*2-3*](*99B*), *Sb*/+ were crossed to *FM7* virgin females. Three hundred lines, each of which was derived from a single nonselected (w^+), mobilized-insertion-carrying chromosome, were established. These were analyzed by Southern blotting with wt genomic DNA flanking the *P842* insertion site as hybridization probes. Several small deletion events which removed flanking DNA but retained the w^+ gene in the original insertion were recovered.

In addition, we took advantage of an interaction between *bif* and *Df*(*2L*)*Prl* to screen for additional mutant alleles of *bif*. *Df*(*2L*)*Prl* is a deficiency which removes the 32F1-3; 33F1-2 cytological interval (10) and acts as a dominant enhancer for the weak rough-eyed phenotype exhibited by loss of function of *bif*. Ethyl methanesulfonate (EMS)-treated *Df*(*2L*)*Prl*/*CyO* males were crossed to virgin females homozygous for a small deficiency, Δ*59* (see Results), which removes *bif*. The resulting heterozygous female progeny (*EMS*/Δ*59*; *Prl*/+; +/+) were scored for eye roughness. The new EMS mutation can be distinguished from Δ*59* because the Δ*59*-carrying chromosome is mutant (w^-) for the *white* gene at its normal cytological position but carries *P842*[(w^+, ry^+)] immediately flanking the deleted sequence; therefore, the newly induced allele can be recovered on a w^- chromosome as a result of recombination in the interval between the newly induced mutation and the mutant *white* gene carried on the Δ*59* chromosome. These new alleles are then checked by Southern blotting to ensure that they do not possess the Δ*59* deletion.

Additional P-element-induced insertion and deletion alleles of *bif* were isolated by mobilizing *P842*. Jump starter females with the genotype w^-, *P842*[(w^+, ry^+)]/w^-; Δ*2-3 Sb*/+ were crossed to *Df*(*2L*)*Prl*/*CyO* males. Male progeny with the genotype w^+/Y; *Df*(*2L*)*Prl*/+ were scored for eye roughness. The rough-eye males selected from this screen were balanced over *FM7* and analyzed by Southern blots. Only deletion mutations which retained the w^+ gene carried on the P element were recovered.

Isolation of *bif* genomic and cDNA clones. Genomic DNA was prepared from the *P842* insertion line by using standard methods. Subcloning of genomic DNA flanking the P-element insertion site from the *P842* insertion line was described by Bahri and Chia (3). The subcloned flanking DNA was used as a probe to screen an EMBL3 wt genomic library (25). Various cloned genomic fragments were used to screen a 12- to 24-h plasmid embryonic cDNA library constructed by Brown and Kafatos (4), as well as λgt11 and λZAPII random primed embryonic cDNA libraries.

For screening, phage plaques or bacterial colonies were replica plated onto nylon membranes, denatured, UV cross-linked, and hybridized overnight to the probe at 65°C in 5× SSCP–5× Denhardt's solution, 100 mg of dextran sulfate per ml–200 μg of denatured salmon sperm DNA per ml (21). The filters were washed three times in 0.1× SSCP–0.1% sodium dodecyl sulfate at 65°C and exposed to Fuji RX X-ray film.

Northern blot and DNA sequencing. Poly(A)$^+$ RNA was prepared by standard methods. Two-microgram RNA samples were separated on formaldehyde-agarose gels and transferred onto nylon membranes for hybridization.

For sequencing, overlapping restriction cDNA fragments were subcloned into M13 and sequenced by using the Sequenase V20 T7 DNA polymerase kit from United States Biochemicals Inc. Both strands were sequenced by using universal M13 and gene-specific primers. The Blast computer program was used to search the nonredundant GenBank, PDB, SwissProt, SPupdate, and PIR databases for sequence homology.

Immunostaining of embryos and eye discs. Anti-Bif antibody was raised in rabbits by using the peptide sequence KMFEEASANRRPRAAHRS (amino acids [aa] 573 to 589). Following incubation of fixed embryos with the primary anti-Bif antibody and the horseradish peroxidase–anti-rabbit antibody, a modified horseradish peroxidase immunocytochemical method was used (22). Staging of embryos was done in accordance with Campos-Ortega and Hartenstein (5). Photographs were taken by using differential interference contrast optics with a Zeiss Axiophot microscope. The specificity of the sera used was confirmed by showing a complete lack of staining in control animals deficient in *bif*.

For immunofluorescence staining, embryos were devitellinized with 80% ethanol in place of methanol. Following incubation with the primary anti-Bif antibody and anti-rabbit antibody, embryos were stained with fluorescein isothiocyanate-streptavidin for 1 h to visualize Bif expression pattern and with tetramethylrhodamine isothiocyanate-phalloidin for 0.5 h to visualize actin. Stained embryos were washed with phosphate buffer-Triton and mounted in Vectar-shield medium for confocal microscopy.

Prior to sectioning, eyes from adult flies were fixed and embedded in Quetol 651 (Electron Microscopy Sciences) in accordance with the published protocol (27). The ultrathin sections were counterstained with lead citrate and examined by transmission electron microscopy.

Pupal eye discs were dissected as previously described (5) and fixed with 4% paraformaldehyde for 30 min on ice. They were stained with anti-Bif antibody and tetramethylrhodamine isothiocyanate-phalloidin. A Bio-Rad 600 confocal microscope was employed to visualize the images.

Nucleotide sequence accession number. The nucleotide sequence of the *bifocal* gene has been submitted to the GenBank database under accession no. AF011791.

RESULTS

Isolation of the *bif* mutation and its rough-eye phenotype. The first *bifocal* mutation resulted from a screen for local transpositions starting with a P transposon, *Is*(*2*)*P842* (14), located in the 10D cytogenetic interval of the *Drosophila* genome. *Is*(*2*)*P842* homozygotes are phenotypically wt. Southern analysis of 300 putative local transposition events (see Materials and Methods) revealed that one of these, Δ*59*, was in fact an ~60-kb deletion which removes the entire coding region of the receptor tyrosine phosphatase gene, *DPTP10D* (26, 33), as well as the genomic region located between the P-element insertion site and *DPTP10D* (Fig. 1). Animals homozygous for Δ*59* are viable and exhibit a weak rough-eye phenotype (Fig. 2).

Close examination of the *bif* rough-eye phenotype revealed defects in ommatidial and bristle organization. In the wt, the external surface of the adult eye consists of a hexagonal array of ~800 facets with bristles projecting from alternate facet vertices (Fig. 2A). In *bif* mutant eyes, adjacent ommatidia are often fused and bristles are short, missing, or duplicated (Fig. 2B). Bristle precursors are largely normal in the mutant, as seen in anti-Cut antibody-stained pupal discs, but the fused ommatidia may be caused by occasional loss of pigment cells (data not shown). Internally, wt adult ommatidia contain eight photoreceptor cells (R1 to R8), each of which projects into the center a light-gathering organelle called the rhabdomere. The eight rhabdomeres have round cross sections and are organized in an asymmetric trapezoidal pattern (Fig. 2C and G). In *bif* mutant ommatidia, the majority of the rhabdomeres have abnormal morphology; they become enlarged, elongated, or frequently split as if the rhabdomere were duplicated (Fig. 2D). Electron micrographs show that what appears to be rhabdomere duplication under an optical microscope is actually a physical split of the mutant rhabdomeres (Fig. 2H and I). To determine whether additional R cells are recruited in *bif* ommatidia, *bif* pupal eye discs were stained with an anti-elav antibody. A normal complement of eight photoreceptor cells occupying their usual positions were found in the mutant ommatidia (Fig. 3E and F).

The *bif* rough-eye phenotype is enhanced by *fas1* loss of function and by loss of two regions of the *Drosophila* genome. A genetic interaction screen was carried out in search of dominant enhancers of the *bif* rough-eye phenotype. In this screen, *bif* female virgins were crossed to males carrying mutations or deficiencies on the second or third chromosome. Male progeny hemizygous for *bif* and heterozygous for an autosomal deficiency or mutation were examined. Two deficiencies, *Df*(*2L*)*Prl* [32F1-3; 33F1-2] and *Df*(*3R*)*p1 4* [90C02-D01; 91A01-02] (7), were found to dominantly enhance the *bif* rough-eye phenotype. Closer examination of the mutant eyes revealed that they also had elongated, malformed rhabdomeres, similar to the phenotype observed in *bif* mutants. However, the enhanced roughness was found to be due to additional loss or irregular arrangement of ommatidia (data not shown). The region uncovered by *Df*(*2L*)*Prl*, which is responsible for the observed dominant enhancement of the phenotype, was further mapped to the interval 32F1-3; 33B2-3.

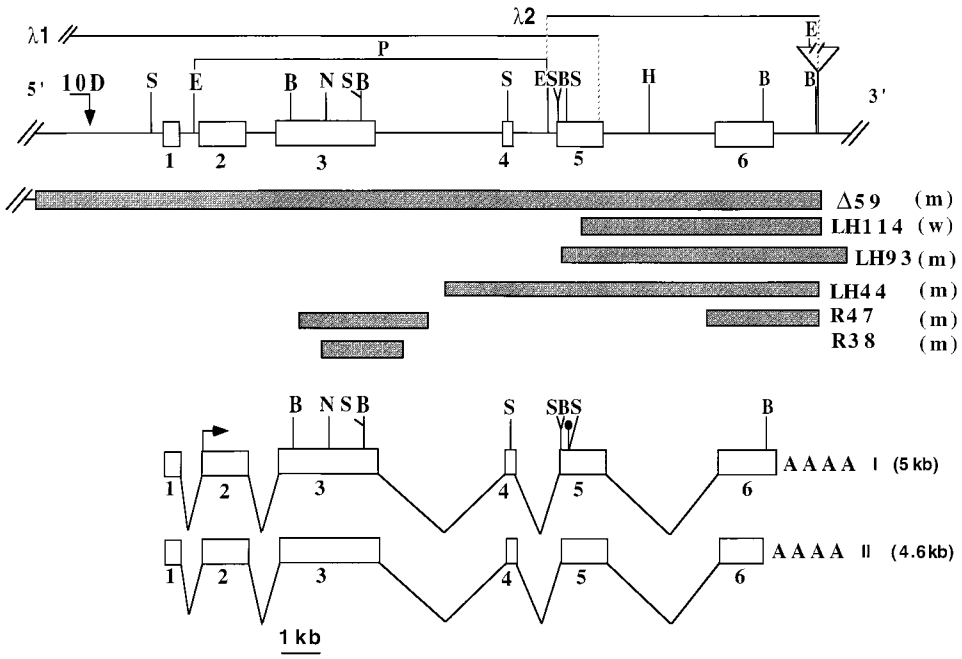

FIG. 1. Schematic representation of the *bif* gene and its transcripts. An abbreviated restriction map of the genomic region encompassing the *bif* transcript is shown on the top line. The two different classes of *bif* cDNAs described in the text are shown, with exons depicted as empty boxes. Exons 1 to 3 were obtained from a random primed embryonic cDNA bank. All other cDNA clones were obtained from embryonic libraries described by Brown and Kafatos (4). The positions of the putative translational initiation and termination sites are indicated as horizontal arrows and solid circles, respectively. The organization of the gene was determined by sequencing the pertinent regions of the genomic DNA and comparing them with the two cDNA sequences. The exons are numbered. Filled rectangles represent deleted sequences in the fly lines *LH114*, *LH37*, *LH44*, *R47*, and *R38*. w, wild-type eye phenotype; m, mutant eye phenotype; S, *Sal*GI; B, *Bam*HI; H, *Hin*dIII; E, *Eco*RI; N, *Not*I. λ1 and λ2 are two genomic DNA clones covering the *bif* gene. P represents the genomic *bif* probe used for cDNA screening and Northern hybridization. The downward-pointing arrow indicates the 3′ end of the *DPTP10D* transcription unit.

The strong rough-eye phenotype of flies homozygous for *bif* and heterozygous for *Df(2L)Prl* is clearly distinguishable from those of animals homozygous for a *bif* null alone. Based on the interaction with *Df(2L)Prl*, additional *bif* alleles were isolated in screens for eye roughness (see Materials and Methods). *R38* and *R47* are two P-element-induced deletion alleles isolated in this screen. They are internal deletions in the *bif* gene (see below) that remove 2 and 3 kb, respectively, from the coding exon 3 regions of *bif* (Fig. 1). The same strategy was also used to isolate four EMS alleles which failed to complement the Δ*59* mutant allele.

In addition, enhancement of the *bif* mutant rough-eye phenotype was observed when generating *bif* males which were also homozygous for the *fas1* mutation. *fas1* encodes a neural cell adhesion molecule (9), and a mutant allele exists which was caused by insertion of a large, transposable element at position 89D (18). Revertant alleles from this insertion which are $fas1^+$ did not enhance the roughness of *bif* mutant eyes. It is interesting that anti-Fas1 antibody stains all photoreceptor cells of the third instar larval eye disc in a pattern similar to that of Bif (data not shown). No obvious defects are seen in homozygous *fas1* eyes. Enhancement of the rough-eye phenotype of *bif* mutant adults was not observed when another neural cell adhesion molecule, *fasIII* (23), was used in the genetic interaction experiment.

Generation of additional *bif* alleles. To determine which sequences deleted in Δ*59* might be responsible for the eye defect, three additional viable P-element-induced deletions (*LH114*, *LH93*, and *LH44*) were isolated (Fig. 1). *LH114* deletes ~6 kb of genomic DNA starting from the P-element insertion site and extending toward, but not into, *DPTP10D*. Flies homozygous for this deletion have wt eyes. However, the overlapping deletion *LH93*, which removes an additional ~0.5 kb of genomic DNA further towards *DPTP10D* produces a rough-eye phenotype. Furthermore, another overlapping deletion, *LH44*, which removes ~9.5 kb of genomic DNA starting from the P-element insertion site and extending toward, but not into, *DPTP10D*, also produces the abnormal eye phenotype. *LH93* and *LH44* do not complement each other, nor do they complement Δ*59* for the eye phenotype. Analysis of these deletions suggested the possibility that *DPTP10D* is not involved; rather, an undefined gene (*bifocal*) located between the *DPTP10D* transcription unit and the *Is(2)P842* insertion site might, in fact, be responsible for the rough-eye phenotype. Lending further support to this view, the other two rough-eye mutations, *R47* and *R38*, which were isolated by taking advantage of a dominant genetic interaction with *Df(2L)Prl*, also remove DNA sequences located between the *DPTP10D* transcription unit and the *Is(2)P842* insertion site (Fig. 1).

***bif* mutations disrupt the open reading frame encoded by a ~5-kb transcript.** To determine whether the region under question harbors an unidentified transcript, an 8.5-kb *Eco*RI genomic DNA fragment which overlaps part or all of the regions deleted in the *LH44*, *R38*, and *R47* mutant alleles (Fig. 1) was used as a probe in a Northern hybridization experiment. The results indicate that this probe hybridizes to several transcripts, the most predominant form of which is ~4.5 kb long (Fig. 3).

Examination of the locations of molecular lesions associated with the various deletions generated by mobilizing *Is(2)842* and the phenotypes they produce strongly supported the view that the open reading frame encoded by the *bif* cDNAs is required for the bif^+ phenotype. *LH114* homozygotes exhibit

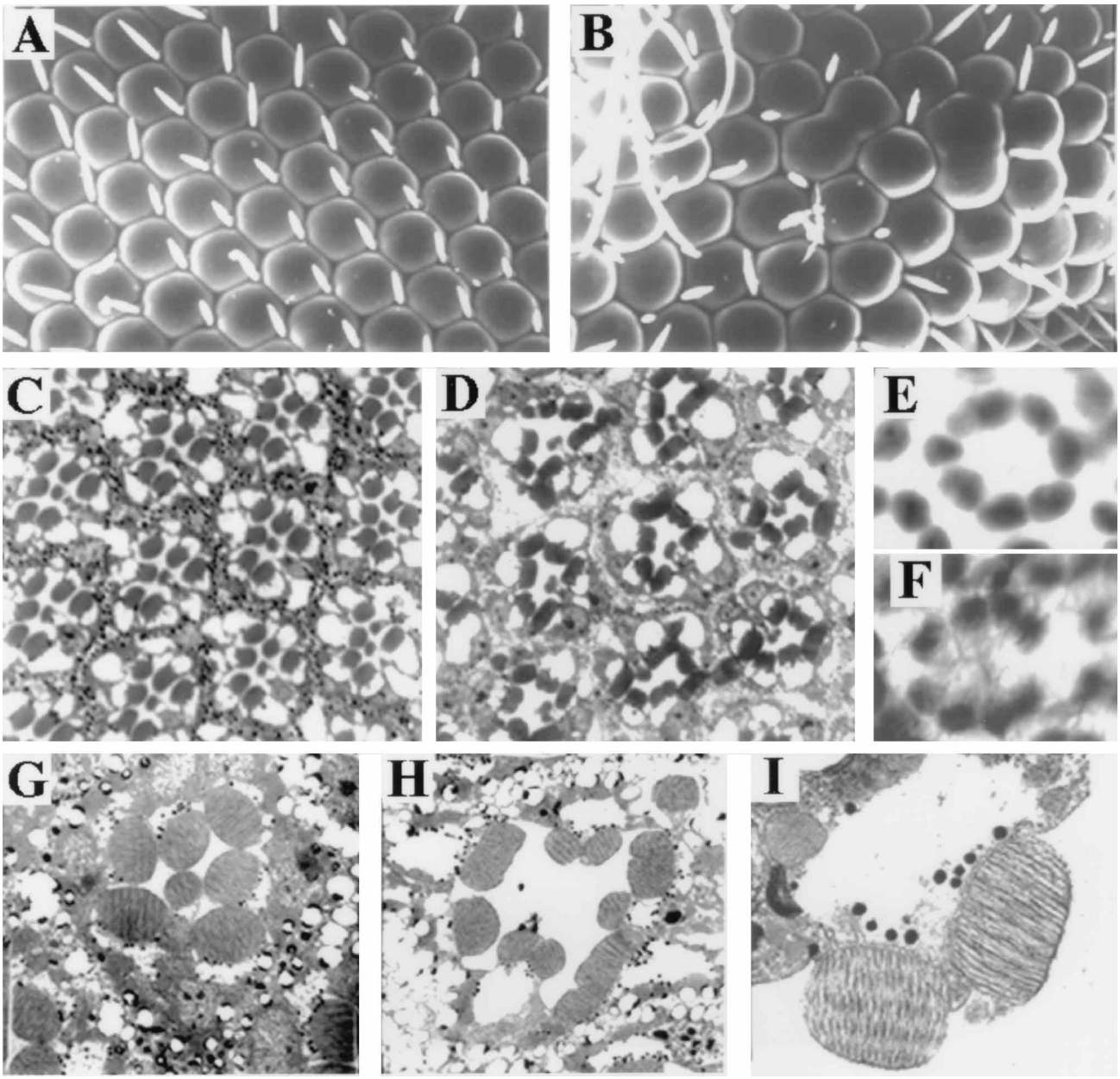

FIG. 2. Phenotype of *bif* mutant eyes. The top panel shows scanning electron micrographs of wt (A) and *bif* null (Δ*59*) mutant (B) adult eyes; note the presence of fused ommatidia and short, often missing bristles in B. (C) Optical section of an *LH114* mutant adult eye showing a wt regular pattern of ommatidia, each containing seven R cells which project their rhabdomeres to the center. (D) Optical section from an adult eye of a *bif* null (Δ*59*) mutant showing disorganized ommatidia with deformed, elongated, and often split rhabdomeres. (E and F) Whole-mount preparations of 50-h wt (C) and *bif* mutant (D) pupal eye discs showing one ommatidium stained with anti-elav antibody, which stains the nuclei of all neurons; both wt and *bif* pupal ommatidia contain eight R cells. G to I are electron micrographs. (G) *LH114* showing a wt ommatidium. (H) Δ*59* mutant ommatidium showing elongated/split rhabdomeres. (I) High magnification of H showing a mutant R4 rhabdomere.

wt eyes; the deletion associated with *LH114* removes sequences from the 3′-flanking and 3′ transcribed nontranslated region of the *bif* cDNAs but leaves the open reading frame intact. In contrast, Δ*59*, *LH93*, *LH44*, *R47*, and *R38*, all of which produce the mutant eye phenotype, are associated with lesions which remove all or part of the open reading frame (Fig. 1). Moreover, with the exception of Δ*59*, none of the mutations appear to affect the expression of the DPTP10D protein (data not shown). These data indicate that it is the new transcription unit associated with the *bif* cDNAs, and not *DPTP10D*, which is responsible for the observed mutant eye phenotype.

bif encodes several transcripts, the most predominant form of which is ~4.5 kb long (Fig. 3). Their expression is differentially regulated during development, with relatively stronger expression in embryos, pupae, and adults and weaker expression in larvae. In the adult head, a larger transcript of ~7 kb is the predominant species. *bif* cDNA clones were isolated by screening embryonic cDNA libraries (see Materials and Methods). They are all related to each other by restriction mapping

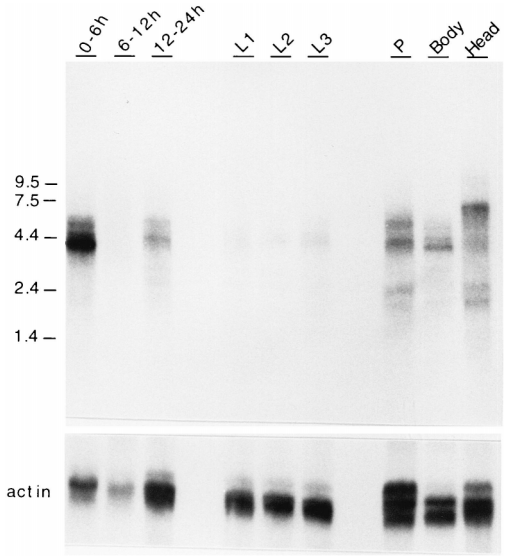

FIG. 3. *bif* transcripts. Northern blot containing 2 μg of poly(A)$^+$ RNA from each of the indicated stages was hybridized to an 8.5-kb *Eco*RI genomic DNA probe containing *bif* exons 2 to 4 (see Fig. 1 legend). 0–6h, 6–12h, and 12–24h indicate the ages of the embryos in hours; 1L, 2L, and 3L are the three different larval stages; P1-2 and P3-4 indicate the ages of pupae in days; Body, adult body; Head, adult head. The lower panel shows the same filter probed with actin. The 6–12h lane is underloaded. Two transcripts of ~4.5 and ~5 kb are detected. The intensity of the 4.5-kb transcript is much higher in the younger embryos (0–6h). An additional *bif* transcript of ~7 kb is detected in the head. The values on the left are molecular sizes in kilobases.

and differ only in the extent of their respective 5′ and 3′ regions. The two largest clones recovered contain inserts of ~4.6 and ~5.2 kb (referred to henceforth as the *bif* cDNAs); these have been sequenced and encode the same open reading frame (see below). Each of these two cDNAs spans >80% of the genomic region between the 3′ end of the *DPTP10D* transcription unit and the *Is(2)P842* insertion site. The major difference between the two species is at their respective 3′ termini, where different polyadenylation sites have been utilized. These two *bif* cDNAs are each comprised of six exons (Fig. 1); they contain the same 3,189-bp open reading frame, which starts with an ATG at nucleotide 305 in exon 2 and ends with a TGA at nucleotide 3493 in exon 5.

bif encodes a putative novel protein of 1,063 aa (Fig. 4) which has no striking homology to any known proteins in the databases searched. Bif is rich in serine/threonine (19.8%) and contains a stretch of 15 glutamine residues at its N terminus (aa 66 to 71). Six of the total of 10 tyrosine residues are concentrated in the C terminus of the Bif protein (aa 916 to 1018). The Prosite search (see Materials and Methods) predicted a possible tyrosine phosphorylation in the sequence ^{908}KSTKEVPDY.

Defects in *bif* rhabdomeres are accompanied by abnormal actin localization. Given the apparent structural cell deformities associated with *bif*, we set out to analyze the eye phenotype at the subcellular level by using antibodies that recognize cytoskeletal markers such as actin, spectrin, and phosphotyrosine. Actin intensely stains the rhabdomeres, whereas phosphotyrosine localizes to the cytoplasmic region adjacent to the rhabdomeral domain of R cells. Spectrin, on the other hand, usually delineates the boundary of the R-cell body. In these studies, the *bif* alleles Δ*59* and *LH44* showed results similar to those obtained with *R47*.

In wt eyes, actin marks the rhabdomeres very early in their development. The star-like staining pattern of actin in the center of the ommatidium at 55 h of pupation is shown in Fig. 5G. At this stage, actin staining is intense in the apical microvillar tips of R cells facing the future interretinal space and is also visible in the smooth stalks extending to the adherens junctions. Proper contacts between these actin-stained apical domains usually ensure normal rhabdomere development (15). In *bif* ommatidia, there is no clear distinction between microvillar tips and stalks at this stage. Instead, the early star-like actin staining becomes abnormal, merging together in the center to form an equator-like pattern (Fig. 5H).

The other two markers used in this study, spectrin and phosphotyrosine, were normally localized in *bif* eye discs (similar to the wt) and did not show any additional morphological disruptions in mutant R cells (data not shown).

Bif and actin appear to be present at similar subcellular locations at various developmental stages. Given the effect that *bif* mutations have on rhabdomeres and the axial actin cytoskeleton, the spatial distribution of Bif relative to that of actin was examined by carrying out double-labelling experiments. The anti-Bif antibody used for this study was raised in rabbits (see Materials and Methods). Since animals null for *bif* are viable, the authenticity of the antibody was ascertained by using the most stringent criteria; i.e., in embryos or eye imaginal discs derived from animals homozygous for the null Δ*59* allele of *bif*, no staining was observed with the serum used for this study.

In the wt, anti-Bif antibody stains all photoreceptor cells as soon as they appear posterior to the morphogenetic furrow in the third instar larval eye disc (Fig. 5A and C). Longitudinal optical sections of the discs show that Bif is apically localized (Fig. 5D and F). At this stage, Bif localization shows a striking resemblance to actin in the developing photoreceptors. Actin is also found in all R cells as visualized by phalloidin staining (Fig. 5B and C) and completely overlaps Bif in the apical

```
                                                                    37
MESQKRPSLDLHTDVPAGLAAGGSGLGAAAEMSPTSG
FLPDMPQWKKDLIQRRKTNVPAPRRVHHLAHRWQLWG
FGRSNAAPGAIADFTEPATISSTSQKRNMIGSEEKSE
KSSISNTNSDSTGGHHSVVAVSLSPDAAATTNVTVTP
IPKQRSSLLNTRSQEREMVRYILSESGERDGELESGE
QPAGVVSNSRCGEVETGTIGSPSSSANQNPNPNHLKT
KCKPGQSVAEGKPSAKETIVDNSKSCSKTKSISDKLQ
SNKFIIQQQQQQQQQQQQQQQLSPTKVTVKPTMVAMQ
EMKKTTKQNGQHRHLAGKIGSVAGGDVDPQHPPTNPI
PDSLDTGEDLSYGPGIVSKLRCRYLSLALRESRQQSS
KQRLQRSTSLNTLLDRDDDEVEVEEPEMTNSQVRAKS
TPPPILGAKPTPKPSSQHQRPVSLGANGAGSAVNPPS
NSDQAQTGAVANGGAGSGQRSRHFKRGNEVMKRARSV
EALLCEKSPWNSQRISTAGAAAAAAPSPPAPKATATA
PSPVTSPTCVTIEDKIHNARERLHSGTDTAPPKRLTS
IIDDTERPPPDLVKQTLKMFEASANRRPRAAHRSNGV
GGVASKVANYKSIIKDQKQPSSAAATPPPTGMGFASS
TPLRHVHPDIIPRQVDSPVSALSVMIARMELQEPETP
ERETRDAEATPQTEALSETERNDRDEGDGEVDDDNHN
NNDDDHDDGDDGSDNNEQRDKMGAAAAGDKPKPPAES
AAGGAQRSFAASTENAHVASGSSSSTSASVRKLSNNN
DSSSGPAVTKQIGVIRPLFNSQGAGSTPLTSREIEKN
RINEMKKSTATDAGGSVSGSGTVAGAGSGTSPTTSLD
SVINTKEAASSETDASASPLWTLRNVRNQSQTAGGGS
GPSSSLHSTENTSMVFNFSKSTKEVPDYIESDVVIYR
RKRELPNGNEPGFVLLGDLSVET<u>**STDTDYDDYSM**</u>CPP
SPCDVEFENANIVIDGKSSIRQKPKESSFRVQFNDTL
TSTFEYPSEASMTIEDPPYADPFGHVSKHHQMLLAEQ
MHLLQHQEQLELEQMHQLGLRRSSTIM    1063
```

FIG. 4. Deduced amino acid sequence of the Bif protein. The amino acid sequence encoded by the open reading frame associated with both of the sequenced full-length *bif* cDNA clones is shown. The single predicted tyrosine phosphorylation site is underlined and in boldface type.

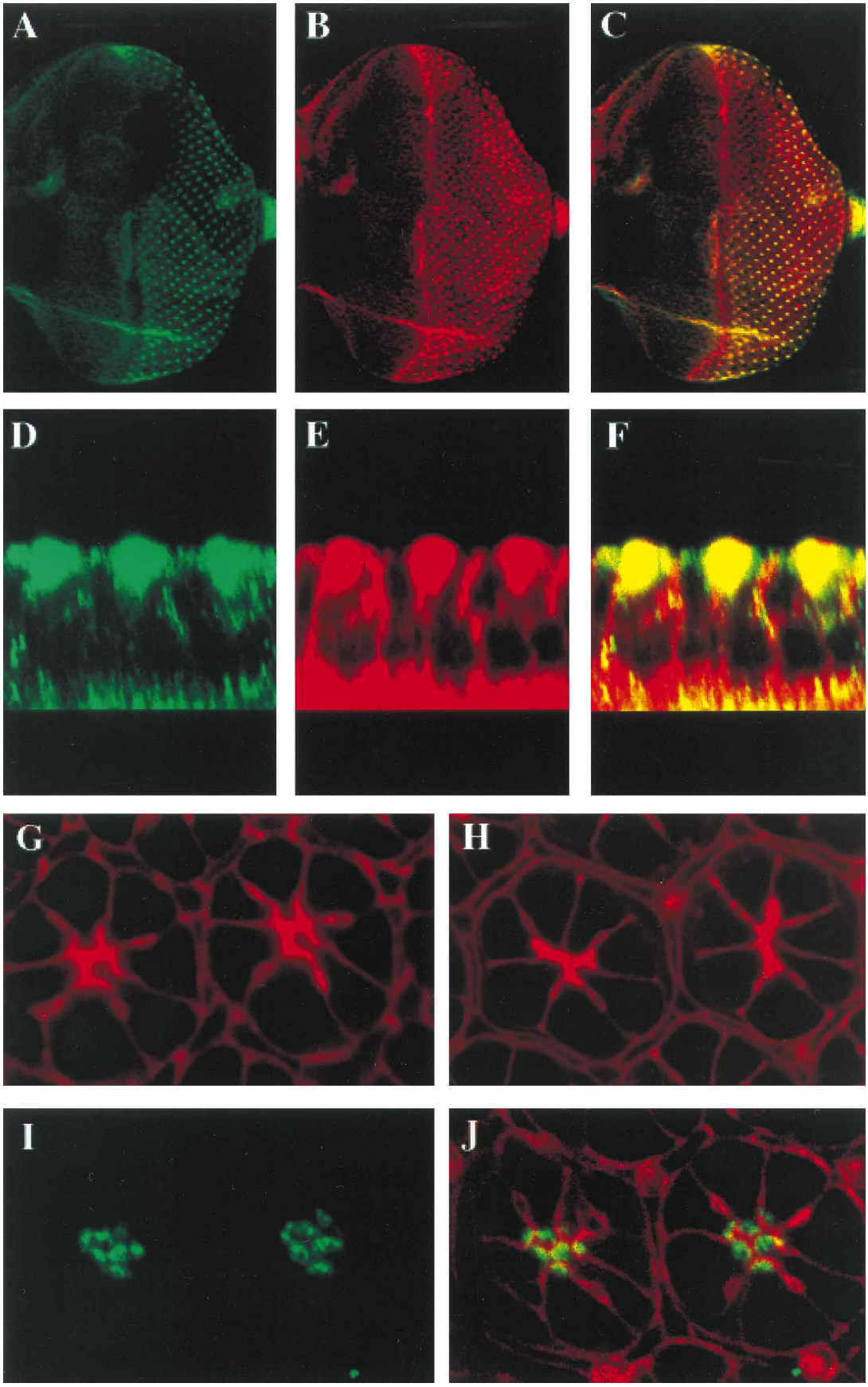
A
B
C
D
E
F
G
H
I
J

FIG. 5. Localization of Bif protein and F actin in larval and pupal eye imaginal discs. (A to C) Confocal images of a whole-mount wt third instar larval eye disc stained with anti-Bifocal antibody (A; staining is in green) and phalloidin (B; staining for F actin is in red). (C) Overlay of A and B showing regions of colocalization for F actin and Bifocal (yellow); anterior is to the left. All R cells posterior to the furrow stain for Bifocal. Bifocal staining is not observed anterior to or within the furrow. D, E, and F are longitudinal optical sections of A, B, and C, respectively; colocalization of both F actin and Bifocal is observed in the apical region of the disc (yellow). G, I, and J are two ommatidia from a wt 55-h pupal eye disc showing the subcellular localization of Bifocal (green; I and J); phalloidin-stained F actin is red (G and J). At this stage, Bifocal and actin only partially overlap (J; yellow). (H) Two ommatidia from a 55-h *bif* mutant pupal eye disc stained with phalloidin showing a disorganized pattern of F actin characteristic of mutant pupal eye discs at this stage.

region (Fig. 5D to F). Both proteins occupy the region where the future rhabdomeres would normally form. Additional actin staining is detected in the morphogenetic furrow. At ~55 h of pupation, Bif becomes localized mainly to the cytoplasmic side of the extending rhabdomeres (Fig. 5I and J). Partial colocalization of the Bif protein with actin can still be seen at this stage, although most of the actin staining is localized to the tip of the rhabdomere (Fig. 5G and J).

Overlapping expression patterns for Bif and actin are also observed during embryogenesis. During the syncytial blastoderm stage, Bif is localized in defined cytoplasmic domains or caps above somatic nuclei and is closely associated with the plasma membrane (Fig. 6). These Bif caps undergo cycle-specific reorganization during each mitosis identical to that of actin (13). Double-labelling experiments show that the expression pattern of Bif just prior to the cellularization stage (nuclear division cycle 14) corresponds to that of F actin and appears in a roughly hexagonal pattern (Fig. 7A, B, and C). The colocalization of both proteins remains throughout cellularization (Fig. 7D, E, and F), and they form rings around the remaining intracellular gaps at the leading edges of the invaginating membrane (30, 31).

Late in embryogenesis, anti-Bif antibody specifically labels the nerve tracts of the central nervous system (CNS) (Fig. 6D to F). Staining is first seen in stage 13 embryos, where the protein seems to be localized primarily on extending neuronal processes and axons. During stage 14, the staining becomes associated with both the anterior and posterior commissures

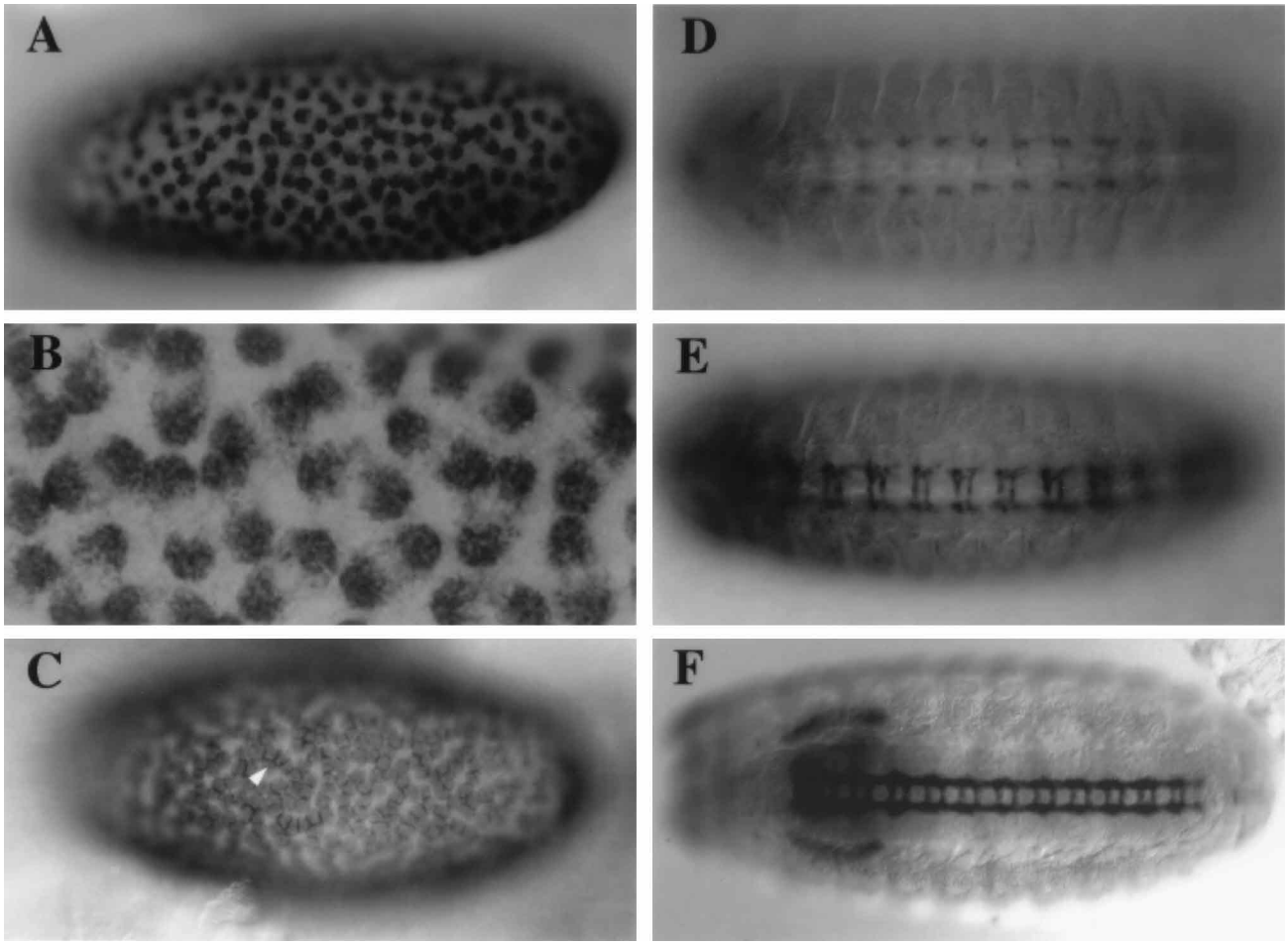

FIG. 6. Bif expression in embryos. Bifocal protein distribution in embryos is very similar to that of F actin. Anterior is to the left. A to C, early preblastoderm stage embryos showing Bifocal staining in cytoplasmic circular caps located immediately underneath the membrane; A, nuclear division 10 stage embryo; B, higher magnification of A showing weak filamentous staining between the separating caps; C, nuclear division 11 stage embryo showing strong Bifocal staining in the regions of contact between adjacent caps (arrowhead). D to F, ventral views of late stage 13 to 16 embryos; D, late stage 13 embryo showing staining in neuropils and axonal projections; E, stage 14 embryo showing staining in anterior and posterior commissures; F, stage 16 embryo showing staining in longitudinal nerve tracts and horizontal commissures of the CNS.

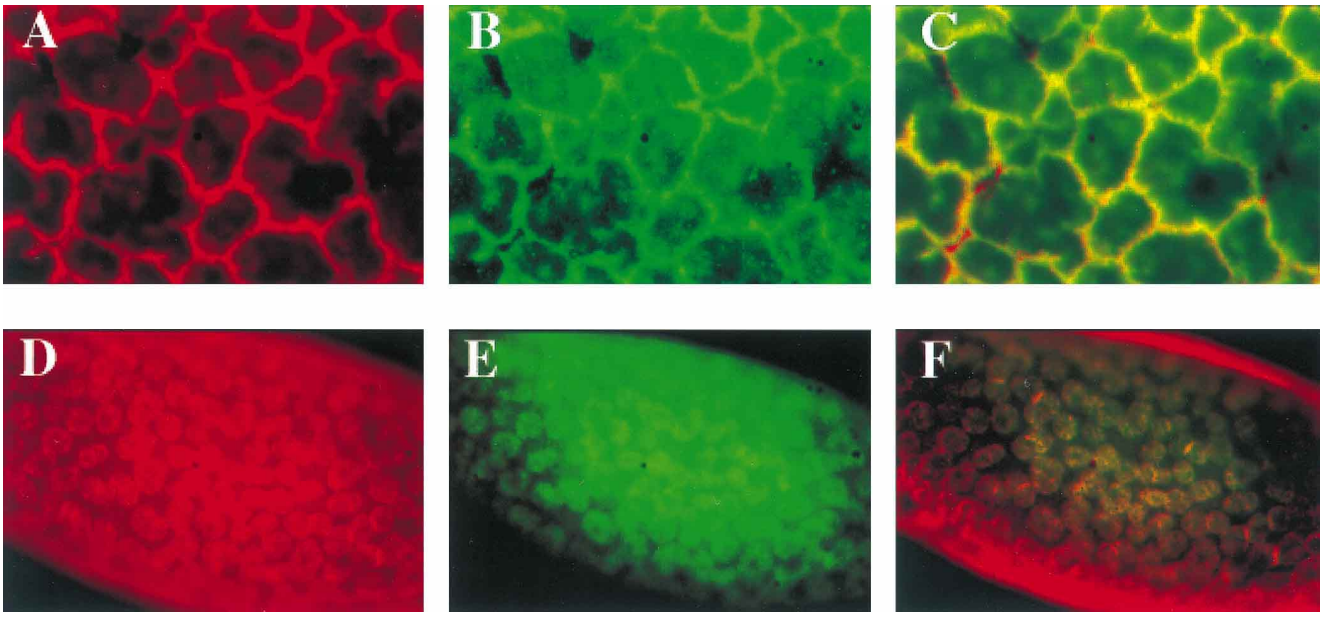

FIG. 7. Bifocal and actin double labelling in embryos. Bifocal is green, and actin is red. A, B, and C show the same embryo at the onset of the cellularization stage stained with phalloidin (A; red) and for Bifocal (B; green). Bifocal and F actin overlap at this stage (C; yellow). D, E, and F are the same embryo toward the end of the cellularization stage showing the persistence of F-actin and Bifocal colocalization.

and later in stage 16 it becomes associated with both commissures and longitudinal connectives of the CNS. Phalloidin-stained actin also labels embryonic CNS axons and shows colocalization with Bif (data not shown).

DISCUSSION

We have cloned and sequenced the *bif* gene, determined its protein distribution, and analyzed the phenotypic consequences of its loss of function during rhabdomere development. *bif* encodes a novel protein which colocalizes with actin during embryogenesis and early during eye development. Phenotypic analysis of null alleles of *bif* indicates that the gene is not essential for viability and has no apparent functional role during embryonic development.

However, during eye development and photoreceptor morphogenesis, Bif is required for the normal formation of actin-rich structures such as rhabdomeres. In the absence of Bif, the distribution of actin becomes abnormal early during the formation of rhabdomeres. This leads consequently to gross morphological defects in the rhabdomeres of adult photoreceptors. These observations suggest that Bif is required for the integrity of the actin-rich rhabdomeres.

Mutation of *bif* does not affect the recruitment of R cells but is required for the development of their actin-rich rhabdomeres. The early expression pattern of Bif in larval R cells remains intriguing. Bif is expressed in the extreme apical region of the cell bodies as soon as they form immediately behind the furrow and long before the initial events associated with rhabdomere development occur, yet there are no obvious deformities in *bif* mutant R cells at this stage. All R cells form normally. This indicates that *bif* is not required for the formation of R cells. It is conceivable that a critical level of Bif must accumulate in the R cell prior to microvillar extension to ensure proper formation of rhabdomeres.

The role of *bif* was established through the analysis of developing R-cell rhabdomeres in normal and *bif* mutant eyes. The formation of actin-rich microvillar rhabdomeres begins at the apical surface of R cells in midpupation. In *bif* mutants, the temporal development of R-cell rhabdomeres is not affected. However, *bif* rhabdomeres start to show a variety of morphological defects during early rhabdomere formation. These deformities were found to be accompanied by aberrations in the actin staining pattern. Bif and actin colocalize in the apical region of R cells (in the third instar larval eye disc), where future rhabdomeres would normally form (in midpupation). In midpupation, most of Bif occupies the cytoplasmic base of the axial actin associated with the forming rhabdomeres along one side of the differentiating R cells. The localization data and the effect on actin distribution suggest that Bif may serve as a cytoplasmic support for the microvillar actin filaments and its presence immediately adjacent to apical membrane folding may confer rigidity on the rapidly expanding cytoplasmic surface. Thus, it appears that the defects of *bif* rhabdomeres reflect a developmental function of the *bif* gene in rhabdomere growth possibly mediated by involvement of the Bif protein in the R-cell cytoskeleton.

The actin-rich cytoskeleton mediates several cellular processes which lead to changes in cell shape, membrane stability, movement, and generation of force. This may involve multiple actin-binding proteins which drive the changes in actin assembly and distribution (for a review, see reference 16). However, in the *Drosophila* eye the stabilizing effect that Bif might have on actin organization may be indirect, as at the molecular level Bif does not contain any obvious actin-binding domain.

Interaction of *bif* with the cell adhesion molecule encoded by *fas1*? The precise nature of the mutations uncovered by the deficiencies that phenotypically interact with *bif* is not known. However, genetic screens can be carried out to isolate interacting genes and therefore allow the identification of their gene products that influence the *bif* mutant phenotype. The interaction of *bif* with *fas1* differs from its interaction with the *Prl* and *p14* deficiencies in that the mutation in *fas1* acts synergistically with *bif* only when both are homozygous. Since Fas1 promotes cell-cell interactions via homophilic binding (9) and

Bif seems to be associated with the R-cell cytoskeleton, it is possible that Bif and Fas1 are involved in maintaining the photoreceptor cytoarchitecture and the overall ommatidial structure.

The *fas1* mutation alone is viable and has no obvious adult eye phenotype, which indicates that this gene may encode a redundant function in the eye. In the embryo, a role for *fas1* in the developing CNS axons was established through its genetic interaction with *abelson* (9). Similarly, the genetic interaction with *bif* provides a basis for the analysis of the functional role that *fas1* may play in eye development.

ACKNOWLEDGMENTS

We thank Don Ready for his comments and advice. We also thank Kathy Matthews and the Bloomington Stock Centre for their help, K. Ray for his help with confocal microscopy, V. Zaman for his help with scanning electron microscopy, and Kai Zinn for the *fas1* mutant allele and revertant. We also thank Sara Zaman, Gerald Udolph, Murni Tio, Thomas Dick, and other members of our laboratory for critical reading of the manuscript and useful discussions.

REFERENCES

1. **Arikawa, K., J. L. Hicks, and D. S. Williams.** 1990. Identification of actin filaments in the rhabdomeral microvilli of *Drosophila* photoreceptors. J. Cell Biol. **110:**1993–1998.
2. **Ashburner, M.** 1989. *Drosophila*: a laboratory manual. Cold Spring Harbor Laboratory Press, Cold Spring Harbor, N.Y.
3. **Bahri, S. M., and W. Chia.** 1994. *DPhK-*γ, a putative *Drosophila* kinase with homology to the vertebrate phosphorylase kinase γ subunits: molecular characterisation and phenotypic analysis of its loss of function. Mol. Gen. Genet. **245:**588–597.
4. **Brown, N. H., and F. C. Kafatos.** 1988. Functional *Drosophila* cDNA libraries from *Drosophila* embryos. J. Mol. Biol. **203:**425–432.
5. **Cagan, R. L., and D. F. Ready.** 1989. The emergence of order in the *Drosophila* pupal retina. Dev. Biol. **136:**346–362.
6. **Campos-Ortega, J. A., and V. Hartenstein.** 1985. The embryonic development of *Drosophila melanogaster*. Springer-Verlag KG, Berlin, Germany.
7. **Detwiler, C., and R. MacIntyre.** 1978. A genetic and developmental analysis of an acid deoxyribonuclease in *Drosophila melanogaster*. Biochem. Genet. **16:**1113–1134.
8. **Drenckhahn, D., and R. Dermietzel.** 1988. Organization of the actin filament cytoskeleton in the intestinal brush border: a quantitative and qualitative immunoelectron microscope study. J. Cell Biol. **107:**1037–1048.
9. **Elkins, T., K. Zinn, L. McAllister, F. M. Hoffmann, and C. S. Goodman.** 1990. Genetic analysis of a *Drosophila* neural cell adhesion molecule: interaction of fasciclin I and Abelson tyrosine kinase mutations. Cell **60:**565–575.
10. **Frei, E., D. Bopp, M. Burri, S. Baumgartner, J. E. Edstrom, and M. Noll.** 1985. Isolation and structural analysis of the extra sex combs gene of *Drosophila*. Cold Spring Harbor Symp. Quant. Biol. **50:**127–134.
11. **Fuchs, R.** 1991. MacPattern: protein pattern searching on the Apple Macintosh. Comput. Appl. Biosci. **7:**105–106.
12. **Hicks, J. L., X. Liu, and D. S. Williams.** 1996. Role of the ninaC proteins in photoreceptor cell structure: ultrastructure of ninaC deletion mutants and binding to actin filaments. Cell Motil. Cytoskeleton **35:**367–379.
13. **Karr, T. L., and B. M. Alberts.** 1986. Organization of the cytoskeleton in early *Drosophila* embryos. J. Cell Biol. **102:**1494–1509.
14. **Levis, R., T. Hazelrigg, and G. M. Rubin.** 1985. Effects of genomic position on the expression of transduced copies of the white gene of *Drosophila*. Science **229:**558–561.
15. **Longley, R. L., Jr., and D. F. Ready.** 1995. Integrins and the development of three dimensional structures in the *Drosophila* compound eye. Dev. Biol. **171:**415–433.
16. **Luna, E. J., and A. L. Hitt.** 1992. Cytoskeleton-plasma membrane interactions. Science **258:**955–964.
17. **Mooseker, M. S.** 1985. Organization, chemistry, and assembly of the cytoskeletal apparatus of the intestinal brush border. Annu. Rev. Cell Biol. **1:**209–241.
18. **Paro, H., M. Goldberg, and W. J. Gehring.** 1983. Molecular analysis of large transposable elements carrying the *white* locus of *Drosophila melanogaster*. EMBO J. **2:**853–860.
19. **Ready, D. F., T. E. Hanson, and S. Benzer.** 1976. Development of the *Drosophila* retina a neurocrystalline lattice. Dev. Biol. **53:**217–240.
20. **Robertson, H. M., C. R. Preston, R. W. Phillis, D. M. Johnson-Schlitz, W. K. Benz, and W. R. Engels.** 1988. A stable source of P-element transposase in *Drosophila melanogaster*. Genetics **118:**461–470.
21. **Sambrook, J., E. F. Fritsch, and T. Maniatis.** 1989. Molecular cloning: a laboratory manual, 2nd ed. Cold Spring Harbor Laboratory Press, Cold Spring Harbor, N.Y.
22. **Shu, S. Y., G. Ju, and L. Z. Fan.** 1988. The glucose oxidase-DAB-nickel method in peroxidase histochemistry of the nervous system. Neurosci. Lett. **85:**69–171.
23. **Snow, P. M., A. J. Bieber, and C. S. Goodman.** 1989. Fasciclin III: a novel homophilic adhesion molecule in *Drosophila*. Cell **59:**313–323.
24. **Steele, F. R., R. Washburn, R. Rieger, and J. E. O'Tousa.** 1992. *Drosophila* retinal degeneration C (rdgC) encodes a novel serine/threonine protein phosphatase. Cell **69:**669–676.
25. **Tamkun, J. W., R. Deuring, M. P. Scott, M. Kissinger, A. M. Pattatucci, T. C. Kaufman, and J. A. Kennison.** 1992. *brahma*: a regulator of *Drosophila* homeotic genes structurally related to the yeast transcription activator SNF2/SW12. Cell **68:**561–572.
26. **Tian, S.-S., P. Tsoulfas, and K. Zinn.** 1991. Three receptor-linked protein-tyrosine phosphatases are selectively expressed on central nervous system axons in the *Drosophila* embryo. Cell **67:**675–685.
27. **Tomlinson, A., and D. F. Ready.** 1987. Cell fate in the *Drosophila* ommatidium. Dev. Biol. **123:**264–275.
28. **Van Vactor, D., Jr., D. E. Krantz, R. Reinke, and S. L. Zipursky.** 1988. Analysis of mutants in chaoptin, a photoreceptor cell-specific glycoprotein in *Drosophila*, reveals its role in cellular morphogenesis. Cell **52:**281–290.
29. **Waddington, C., and M. Perry.** 1960. The ultrastructure of the developing eye of *Drosophila*. Proc. R. Soc. London B Biol. Sci. **153:**155–178.
30. **Warn, R. M., and R. Magrath.** 1983. F-actin distribution during the cellularization of the *Drosophila* embryo visualized with FL-phalloidin. Exp. Cell Res. **143:**103–114.
31. **Warn, R. M., and M. Robert-Nicoud.** 1990. F-actin organization during the cellularization of the *Drosophila* embryo as revealed with a confocal laser scanning microscope. J. Cell Sci. **96:**35–42.
32. **Wolf, T., and D. F. Ready.** 1993. Pattern formation in the *Drosophila* retina, p. 1277–1325. *In* M. Bate and A. Martinez-Arias (ed.), The development of *Drosophila melanogaster*, vol. 2. Cold Spring Harbor Laboratory Press, Cold Spring Harbor, N.Y.
33. **Yang, X., K. T. Seow, S. M. Bahri, S. H. Oon, and W. Chia.** 1991. Two *Drosophila* receptor-like tyrosine phosphatase genes are expressed in a subset of developing axons and pioneer neurons in the embryonic CNS. Cell **67:**661–673.
34. **Yang, Y., and D. Ballinger.** 1994. Mutations in *calphotin*, the gene encoding a *Drosophila* photoreceptor cell-specific calcium-binding protein, reveal roles in cellular morphogenesis and survival. Genetics **138:**413–421.